Transmission of terahertz wave through one-dimensional photonic crystals containing single and multiple metallic defects

Hai-Ying Liu,[1] Sen Liang,[1] Qiao-Feng Dai,[1] Li-Jun Wu,[1] Sheng Lan,[1,a)]
Achanta Venu Gopal,[2] Vyacheslav A. Trofimov,[3] and Tatiana M. Lysak[3]
[1]*Laboratory of Photonic Information Technology, School of Information and Optoelectronic Science and Engineering, South China Normal University, Guangzhou 510006, People's Republic of China*
[2]*Department of Condensed Matter Physics and Material Science, Tata Institute of Fundamental Research, Homi Bhabha Road, Mumbai 400005, India*
[3]*Department of Computational Mathematics and Cybernetics, M. V. Lomonosov Moscow State University, Moscow 119992, Russia*

(Received 12 January 2011; accepted 24 August 2011; published online 3 October 2011)

We investigated numerically and experimentally the transmission of terahertz (THz) waves through single and multiple metallic defects created in a one-dimensional (1D) photonic crystal (PC) by inserting single metallic wires or arrays of parallel metallic wires into the air-gap defect of the 1D PC. The transmission properties of the metallic defect modes generated in the photonic bandgap (PBG) were characterized by using THz time-domain spectroscopy. For single metallic defects, it was found that the appearance the defect mode depends not only on the diameter of the metallic wires but also on the polarization of the THz wave. For transverse magnetic (TM) polarized waves whose electric fields are parallel to the metallic wires, the incident THz wave is generally split into two identical parts. In sharp contrast, the excitation of surface plasmon polaritons (SPPs) with enhanced field intensity is observed for transverse electric (TE) polarized waves whose electric fields are perpendicular to the metallic wires. In both cases, two resonant modes with reduced transmittance are observed in the PBG. While the resonant mode related to SPPs is found at the long-wavelength side of the original defect mode, the resonant mode without the excitation of SPPs appears at the short-wavelength side. Numerical simulation based on the finite-difference time-domain (FDTD) technique revealed that the electric field of SPPs is more tightly confined at the surface of the metallic wire when it is placed in the PC, implying that the confinement of a THz wave in the propagation direction will facilitate the localization of SPPs in the transverse direction. For two parallel metallic wires, the defect mode was found to depend on the separation between them. If they are widely separated, then the excitation of SPPs is similar to that observed in single metallic wires. However, the excitation of dipole-like SPPs does not occur for two closely packed metallic wires because of their large lateral size. It was also revealed that two parallel metallic wires with a small diameter and a narrow separation could be employed to achieve a significant enhancement, as large as 21.6, for the electric field in between them. More interestingly, the enhancement factor becomes larger when the confinement of the electric field in the propagation direction is increased. For an array of four widely separated wires whose lateral dimension is wider than the diameter of the THz beam, only one resonant mode is observed at the long-wavelength side of the original defect mode. The experimental observations are in good agreement with the simulation results based on the FDTD technique. The enhanced concentration of the electric field of SPPs at the surfaces of metallic defects may be useful for focusing and sensing of THz waves. [doi:10.1063/1.3642994]

I. INTRODUCTION

Photonic crystals (PCs), which are periodic modulations of dielectric constant or refractive index, have been extensively investigated because of their potential applications in the construction of various functional devices in the last two decades.[1,2] In most cases, defects are intentionally introduced into a PC through modifying the physical properties of certain elements in the PC (e.g., size or refractive index) or breaking the translation symmetry of the PC.[1,2] The defects created in this way can function as cavities or resonators that are important for engineering the spontaneous emission of atoms. On the other hand, PC cavities like this can be employed to construct passive and active optical components such as optical filters,[3] optical delay elements,[4–6] and even optical switches[7–10] and optical limiters[11] when nonlinearity is introduced into the cavities.

Fabrication and characterization of PCs operating in the optical wavelength region is not easy because of the small feature size of the constituent elements in PCs. Fortunately, the scaling property of PCs enables the examination and investigation of their physical properties in the longer wavelength region (e.g., in the microwave or THz spectral

a)Author to whom correspondence should be addressed. Electronic mail: slan@scnu.edu.cn.

region).[1,2] Because of the relatively large feature size, PCs in the THz spectral region can be easily constructed and they offer us the opportunity to investigate the physical properties of PCs that are not easily accessible in the optical wavelength region. Therefore, the construction of PCs in the THz spectral region and the fabrication of functional devices based on such PCs have been theoretically studied and experimentally demonstrated, including filters,[12,13] cavities,[14] waveguides,[15] sensors,[16] switches,[17,18] and so on. In these devices, dielectric defects whose refractive indices can be externally controlled or adjusted are employed to realize various functions. The transmission properties of THz wave through these defect modes were characterized by THz time-domain spectroscopy (THz-TDS).[19,20] However, a systematic investigation of the transmission properties of the metallic defects created in PCs is still lacking.

Physically, the transmission of an incident wave through the defect in a PC is considered as a resonant tunneling of photons through a double-barrier structure. This process involves the excitation of the defect mode. For dielectric defects, the field distributions of the defect modes can be classified into monopole, dipole, and multipole distributions, depending on the size of the defect.[21] Also, it is well known that the resonant frequency of the defect mode can be modified by simply changing the size of the defect.[21] For metallic defects, however, the situation is complicated by the unique dispersion of metals and the excitation of surface plasmon polaritons (SPPs).

In the THz spectral region, metals resemble in many ways a perfect conductor, and negligible penetration of the electromagnetic fields into metals leads to highly delocalized SPPs.[22] These kinds of delocalized SPPs are unique because they permit efficient energy transfer into the far field while preserving the coherence of the electromagnetic field.[23] It has been demonstrated that the electromagnetic wave can coherently transmit through dense three-dimensional (3D) random media composed of subwavelength size metallic particles.[23,24] Despite the subwavelength heterogeneity scale, significant electromagnetic energy is transported across the extent of the medium, which can exceed the bulk absorption depth up to 5 orders of magnitude.[23] The preservation of the radiation polarization state in addition to strong dispersion of the transmitted pulses suggests that the transmission is mediated by near-field coupling of resonant surface plasmon modes and in this case the 3D random medium can be considered as a dielectric material characterized by an effective dielectric constant.[24] It is also indicated that the excitation of dipole-like SPPs in metallic particles whose diameter is smaller than a critical value is crucial for realizing the efficient and coherent transmission of the electromagnetic wave.[25]

In this article, we investigate numerically and experimentally the transmission of THz waves through single and multiple metallic defects created in a 1D PC by inserting single metallic wires or arrays of parallel metallic wires into the air-gap defect of the 1D PC. The paper is organized as follows. In Sec. II, we describe the fabrication of 1D PCs in the THz spectral region and the experimental setup used to implement THz-TDS. Then, the numerical simulation based on the finite-difference time-domain (FDTD) technique is introduced in Sec. III. In Secs. IV and V, the physical properties of metallic defect modes created by single metallic wires and two parallel metallic wires are presented, respectively. The metallic defect mode generated by an array of four parallel metallic wires is discussed in Sec. VI. Finally, a summary of our research work is given in the conclusion.

II. FABRICATION OF 1 D PCS AND EXPERIMENTAL SETUP FOR THZ-TDS

As mentioned above, PCs with photonic bandgaps (PBGs) in the THz spectral region are easily fabricated because of their large feature size. In this study, we chose conventional glass cover slides made of BK7 glass to construct 1D PCs, for three reasons. First, the absorption of BK7 glass is quite small in the THz spectral region. Second, its refractive index appears to be much larger in the THz spectral region than that in the optical wavelength region. This feature enables the construction of PCs with wider and deeper PBGs. Finally, the dispersion of BK7 glass is negligible in the THz spectral region. The refractive index of BK7 glass measured by THz-TDS is about 2.5 in the THz spectral region.[26]

The 1D PCs used in our study were created by combining two stacks of glass slides. They were fabricated by stacking 170 μm thick glass slides one by one with a 50 μm thick plastic film in between the two neighboring glass slides. Once the glass slides were fixed by curing agent at the edges, all the plastic films were removed, leaving a 50 μm thick air gap in between the two neighboring glass slides. With these structure parameters, the first PBGs of the 1D PCs are located at the peak frequency of our THz source which is about 0.30 THz. An air-gap defect can be easily introduced into the PBG by adjusting the separation between the two stacks. On the basis of our previous study,[26] we set the separation between the two stacks at 450 μm, as schematically shown in Fig. 1. In this case, the resonant wavelength of the air-gap defect appears at the center of the PBG ($\sim$0.29 THz) and the space between two stacks is sufficient for the insertion of metallic wires whose diameter is about 300 μm.

The experimental setup for THz-TDS is similar to those reported previously.[19,20,26] The 800 nm laser pulses (130 fs and 76 MHz) from a Ti:sapphire oscillator (Mira 900, Coherent) pumped with a solid-state laser (Verdi-5, Coherent) are split into two beams by a beam splitter. One beam is used to excite the photoconductor antenna of the THz emitter

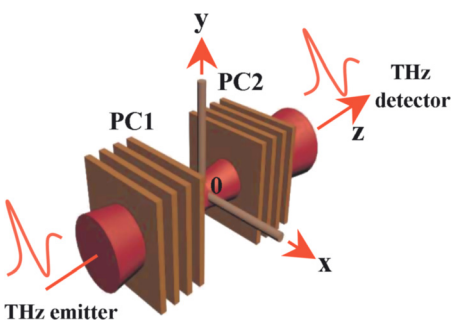

FIG. 1. (Color online) Schematic showing the creation of metallic defects in a 1D PC by inserting a single metallic wire (or an array of parallel metallic wires) into the air-gap defect of the PC and the characterization of the metallic defect modes by THz-TDS measurements.

(Expla Company) and the other is used to trigger the THz detector (Expla Company). The generated THz beam is collimated and focused by four parabolic mirrors arranged in 8-F confocal geometry, providing effective beam coupling between the emitter and the detector. The THz beam is focused to a frequency-independent beam with a waist of ~3.5 mm where the sample is located. For convenience, we choose the beam center at the waist as the origin and establish a coordinate system as depicted in Fig. 1. The propagation direction of the THz wave is chosen as the z axis while the horizontal and vertical directions are set as the x and y axes, respectively. In our experiments, the polarization of the incident THz wave from the emitter was along the y axis. In this case, the incident THz wave behaved as a TE-polarized (electric field perpendicular to the metallic wire) or a TM-polarized wave (electric field parallel to the metallic wire) when a single metallic wire (or an array of parallel metallic wires) was inserted into the defect horizontally or vertically, as shown in Fig. 1. The output signal from the detector is fed into a lock-in amplifier (SR830, Stanford Research Systems) whose output is recorded by a Labview-based data acquisition system. In THz-TDS measurements, the time extent of the terahertz pulse scans was chosen to be 102.4 ps (1024 measurement points with a time step of 0.1 ps). To clearly resolve the defect mode with a narrow linewidth, however, zero padding to 409.6 ps was employed, giving a frequency resolution of ~2.5 GHz. This method has been generally used to improve the frequency resolution through interpolation between measured frequency points.[19,27,28] We performed THz-TDS measurements directly in air instead of in a plastic box filled with nitrogen, for two reasons. First, the first PBG of the 1D PC is designed at the peak frequency of the THz source (~0.30 THz), which is below the first absorption peak of water vapor. Second, the insertion of metallic wires becomes easier without the use of the box.

III. NUMERICAL SIMULATION METHOD

In order to gain a deep insight into the propagation of THz waves through various defects, numerical simulations based on the FDTD technique were carried out for two-dimensional (2D) PCs containing various metallic defects, to obtain the transmission spectra and field distributions of the metallic defect modes.[29] In all cases, a perfectly matched layer boundary was employed to ensure negligible reflection at the boundaries. The grid sizes in both the y and z directions were chosen to be 5 μm, which is about 1/200 of the central wavelength of the ultrashort THz pulses used in the experiments ($\lambda \sim 1000$ μm). When calculating the transmission spectra, continuous waves with Gaussian distributions were incident on the PCs and the transmitted powers were detected by power monitors placed behind the PCs.

IV. METALLIC DEFECT MODES FORMED BY SINGLE METALLIC WIRES: NUMERICAL SIMULATION AND EXPERIMENT

In general, it is thought that the physical properties of metallic defects are governed by both the dispersion relation of the metal and the excitation of SPPs.

First, let us see by numerical simulation the transmission spectrum of the 1D PC containing a metallic defect formed by inserting a metallic wire with a diameter of 300 μm into the air-gap defect of the PC. In the THz spectral region, the difference in dispersion for most metals is not large. For simplicity, the dispersion of the metal in the THz spectral region is chosen to be that of gold $\varepsilon(\omega) = \varepsilon_\infty - \frac{\omega_p^2}{\omega(\omega+i\gamma)}$, where $\varepsilon_\infty = 1$, $\omega_p = 1.37 \times 10^4$ THz and $\gamma = 40.7$ THz.[30] The transmission spectra of the PCs with metallic defects are shown in Fig. 2 for TE- and TM-polarized waves. Here, TE polarization means that the electric field of the THz wave is perpendicular to the metallic wire. For comparison, the transmission spectrum of the PC without metallic defect is also provided. In both cases, two resonant modes are observed. For TE-polarized waves, one resonant mode appears at the long-wavelength side of the original defect mode while the other is located at the short-wavelength side. For TM-polarized waves, the two resonant modes are found at the short-wavelength side of the original defect mode. This phenomenon is completely different from what one observes when a dielectric rod is inserted into the defect region. In that case, only a shift of the defect mode to a longer wavelength is observed. It is also noticed that for both TE- and TM-polarized waves the transmittance of the resonant modes is reduced to some extent as compared with the original defect mode.

In order to find out the physical origin for the formation of metallic defect modes, the distributions of the electric field in the defect region have been calculated, and they are shown in Figs. 3 and 4 for TE- and TM-polarized waves, respectively. For TE-polarized waves, we can see that the field distributions for the two resonant modes are much different. For the resonant mode at 1025 μm, the incident wave is split into two identical parts whose electric field distributions look like those of the original defect mode. For the resonant mode at 1105 μm, however, we observe a dipole-like field distribution with a large field enhancement at the surface of the metallic wire. The maximum field intensity at the surface of the metallic wire is almost five times larger than that observed in the resonant mode at 1025 μm. When a metallic wire is illuminated by an electromagnetic wave, it is

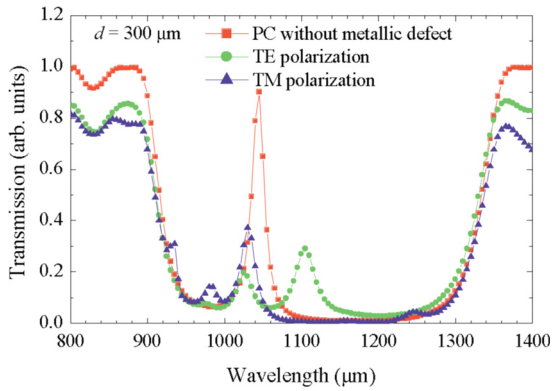

FIG. 2. (Color online) Calculated transmission spectra of the PC containing a 300 μm diameter metallic wire for TE- and TM-polarized waves. The transmission spectrum of the PC without metallic wire is also provided for reference.

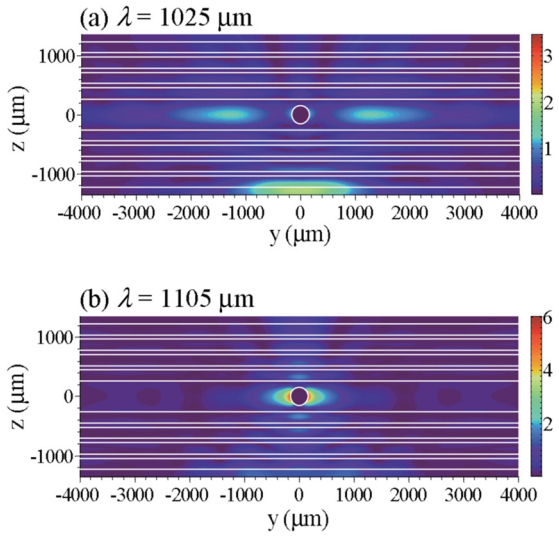

FIG. 3. (Color online) Calculated electric field distributions of the two resonant modes located at 1025 μm (a) and 1105 μm (b) for TE-polarized waves.

possible to excite SPPs with a dipole-like field distribution provided that the diameter of the wire is smaller than a certain value.[25] With increasing diameter, however, the field distribution is changed to a multipole one. It is remarkable that the field enhancement at the surface of the metallic wire becomes larger and the electric field of SPPs is more tightly confined at the surface of the metallic wire when the excitation of SPPs occurs in the defect of a PC. In Fig. 5, we compare the transverse electric field distribution of SPPs along the y axis for a 300 μm diameter metallic wire excited in air and in the PC. It can be seen that the maximum electric field, which appears at the surface of the metallic wire, is enhanced from 1.4 to 6.09. In addition, the confinement of the electric field, which can be characterized by the decay length of the electric field (i.e., the length at which the electric field is reduced to be 1/e of the maximum value), is significantly reduced from 1065 μm to 350 μm. Numerical simulations

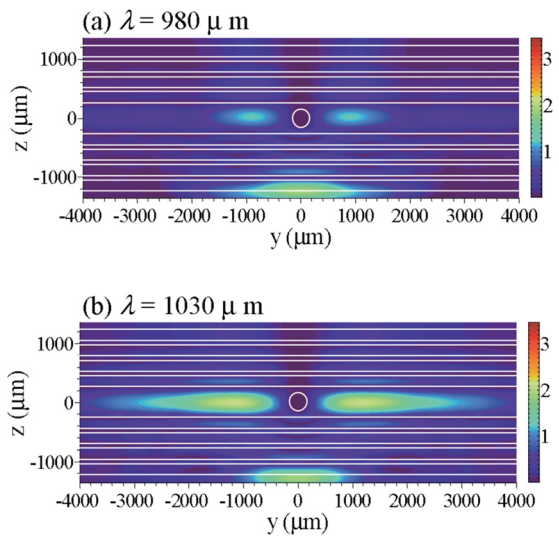

FIG. 4. (Color online) Calculated electric field distributions of the two resonant modes located at 980 μm (a) and 1030 μm (b) for TM-polarized waves.

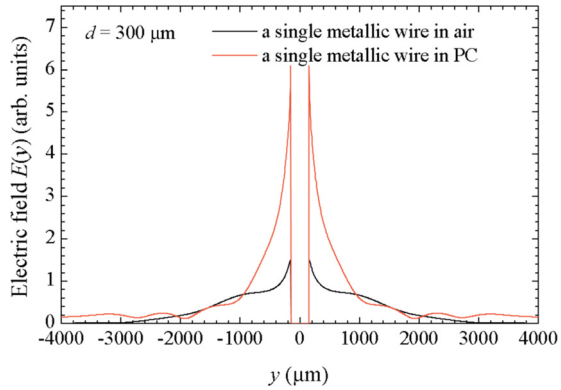

FIG. 5. (Color online) Comparison of the electric field (along the y axis) of the SPPs of the resonant mode at 1105 μm for TE-polarized waves excited in air and in the PC.

also reveal that the electric field at the resonant wavelength is increased from 3.51 for a four-layer $(2+2)$ PC to 4.99 and 6.09 for six-layer $(3+3)$ and eight-layer $(4+4)$ PCs, respectively. This implies that the squeeze of the electric field in the propagation direction will facilitate the concentration of the electric field in the transverse direction.

For TM-polarized waves, the electric field distribution of the resonant mode at 1030 μm appears to be similar to the resonant mode of TE-polarized waves at 1025 μm. For the resonant mode at 980 μm, the field intensity becomes more concentrated on both sides of the metallic wire but the transmittance is much smaller, as can be seen in Fig. 4.

In experiments, we used a stainless steel wire with a diameter of $d = 300$ μm. It was fixed on a 3D microdisplacement stage and gradually inserted into the defect (i.e., the air gap) of the 1D PC. In order to see the effect of SPPs, the metallic wire was inserted into the defect along both horizontal and vertical directions, as schematically shown in Fig. 1. Because the THz wave was vertically polarized in our experimental setup, it is expected that SPPs would be excited when the metallic wire was inserted into the defect horizontally. In Fig. 6(a), we present the transmission spectra of the 1D PC containing the single metallic defect for TE- and TM-polarized waves. The transmission spectrum of the 1 D PC without metallic defect is also provided for reference. The phase of the transmitted wave is shown in Fig. 6(b). For TM-polarized waves, a resonant mode with a reduced transmittance appears at the short-wavelength side of the original defect mode. The other resonant mode observed in the numerical simulation cannot be identified due to its small transmittance. For TE-polarized waves, two resonant modes can be seen in the transmission spectrum. One appears at the short-wavelength side of the original defect mode while the other appears at the long-wavelength side. The situation is similar to that observed in the numerical simulation and the measured resonant wavelengths coincide with those obtained by numerical simulation. The resonant mode appearing at ~1105 nm involves the excitation of SPPs and its electric field distribution is shown in Figs. 3 and 5. Another remarkable feature is the change of the phase appeared only in the wavelength region between the two resonant modes, as shown in Fig. 6(b).

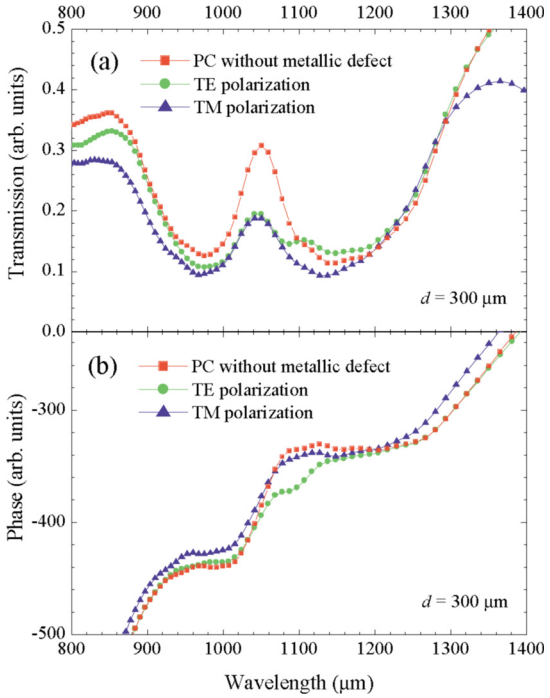

FIG. 6. (Color online) Measured transmission spectra (a) and the phase spectra (b) of the PC without and with a 300 μm diameter metallic wire for both TE- and TM-polarized waves.

In the experiments and simulations described above, we have employed a metallic wire with a diameter of $d = 300$ μm to create metallic defect mode and observed the splitting of the original defect mode into two resonant modes for TE-polarized waves. Particularly, the resonant mode at long wavelength involves the excitation of SPPs. A detailed investigation reveals that the separation between the two resonant modes depends strongly on the diameter of the metallic wire. The bigger the metallic wire, the larger the separation is. The evolution of the two resonant defect modes with increasing diameter of the metallic wire, calculated by numerical simulation is shown in Fig. 7. While the resonant mode at short wavelength remains nearly unchanged, the resonant mode at long wavelength is found to shift to longer wavelengths with increasing diameter of the metallic wire. In addition, the Q factor, which is defined as the ratio of the central wavelength of the defect mode to the full width of the defect mode at half maximum, decreases when the diameter of the metallic wire is increased. They are calculated to be 52.8, 40.0, 29.9, and 26.8 for $d = 100$, 200, 300, and 400 μm, respectively.

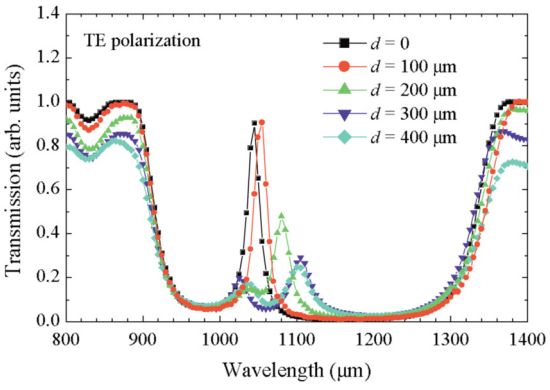

FIG. 7. (Color online) Evolution of the transmission spectrum of the PC with increasing diameter of the metallic wire for TE-polarized waves.

V. METALLIC DEFECT MODES FORMED BY TWO PARALLEL METALLIC WIRES: NUMERICAL SIMULATION AND EXPERIMENT

In the last section, it has been shown that metallic defect modes can be created by simply inserting a metallic wire into the air-gap defect of the 1D PC. TE-polarized waves can transmit the metallic defect through a resonant mode involving the excitation of SPPs. It is interesting to know the transmission properties of metallic defects composed of two or more metallic wires. To do so, we have inserted two 300 μm diameter metallic wires that are separated widely ($w \sim 1.0$ mm) into the defect region. The transmission spectra of the 1D PC containing such metallic defects are shown in Fig. 8 for both TE- and TM-polarized waves. Again, the transmission spectrum of the 1D PC without a metallic defect is also plotted for reference. It can be seen that the appearance of metallic defect modes is quite similar to that observed in a single metallic defect. It implies that there is no coupling between the two metallic defects. The resonant mode related to the excitation of SPPs appears at a longer wavelength of $\sim$1150 μm. It becomes more apparent as compared with the case of single metallic defects.

The transmission spectrum of the 1D PC containing two parallel metallic wires for TE-polarized waves calculated by numerical simulation is shown in Fig. 9. For comparison, the transmission spectra for the PCs without and with a single metallic wire are also provided. As compared to the case of a single metallic wire, one can find an increased attenuation of the resonant mode at short wavelengths and an enhanced transmittance for the resonant mode at long wavelengths. Actually, one can identify three resonant modes in the transmission spectrum of the 1D PC with two metallic wires, as indicated by the arrows in Fig. 9. They are located at 980, 1022, and 1113 μm, respectively. The electric field distributions for these defect modes are shown in Fig. 10. It is apparent that only the defect mode located at 1113 μm involves the excitation of SPPs and produces a strong electric field in between the two metallic wires.

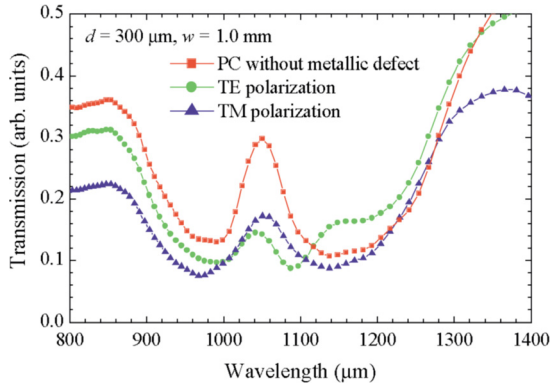

FIG. 8. (Color online) Measured transmission spectra of the PC containing two parallel metallic wires ($d = 300$ μm) separated by 1 mm for TE- and TM-polarized waves.

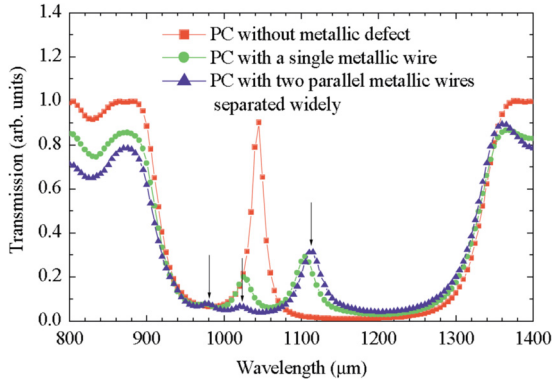

FIG. 9. (Color online) Calculated transmission spectra of the PC containing two parallel metallic wires ($d = 300$ μm) separated by 1 mm for TE-polarized waves. For comparison, the transmission spectra without and with a single metallic wire are also provided.

By numerical simulation, it is also found that a large enhancement in field intensity can be achieved by using two parallel metallic wires with a smaller size and a narrower separation. Figure 11(a) shows the electric field distribution of two 100 μm diameter metallic wires separated by only 50 μm. Field enhancement as large as $\sim$16.6 can be obtained at the center, between the two wires. Furthermore, it is also found that the field enhancement factor can be further increased to $\sim$21.6 by using a twelve $(6+6)$-layer PC. In Fig. 11(b), we present the calculated transverse electric field distributions for the two metallic wires placed in air and in the PC. The electric field intensity is enhanced dramatically from 1.9 to 16.6. In addition, the decay length of the electric field is reduced from 780 μm to 330 μm, indicating a tighter confinement of electric field when the two metallic wires are placed in the PC.

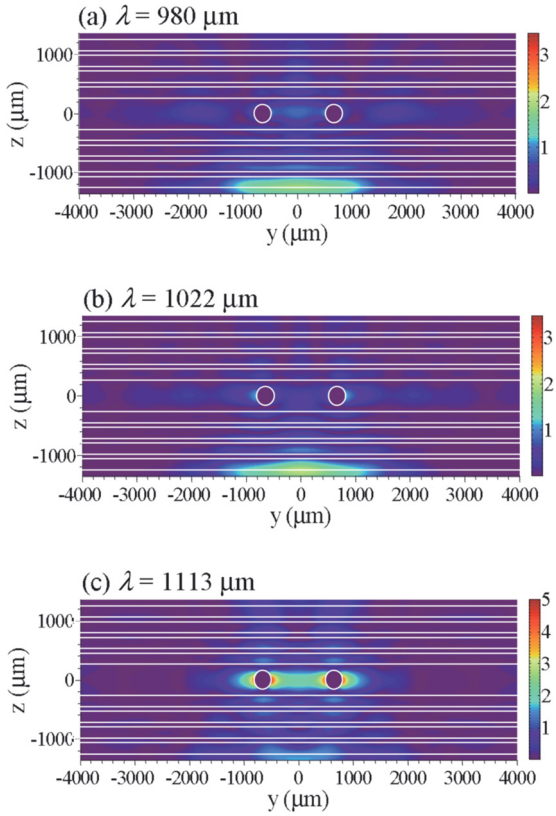

FIG. 10. (Color online) Calculated electric field distributions of the three resonant modes located at 980 μm (a), 1022 μm (b), and 1113 μm (c) for the PC containing two parallel metallic wires ($d = 300$ μm) separated by 1 mm for TE-polarized waves.

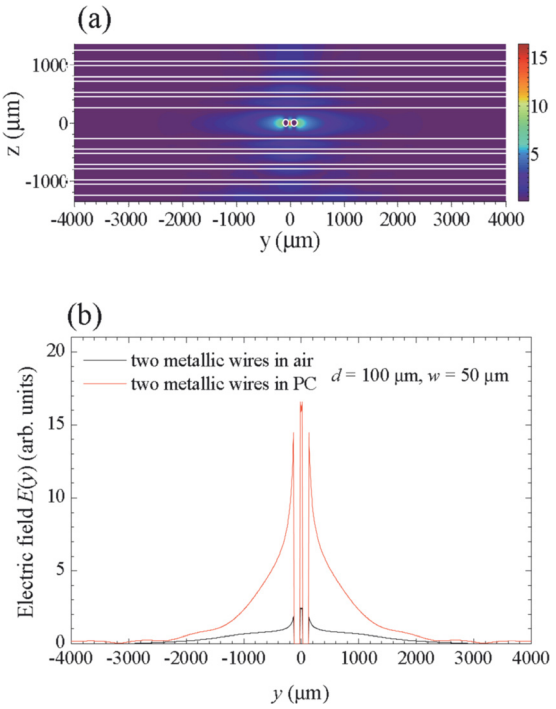

FIG. 11. (Color online) (a) Calculated electric field distribution of the PC containing two 100 μm diameter metallic wires separated by 150 μm for TE-polarized waves. (b) Comparison of the electric field (along the y axis) of the SPPs of the resonant mode excited in air and in the PC.

Apart from the two widely separated metallic wires, it is also interesting to find out the transmission properties of two

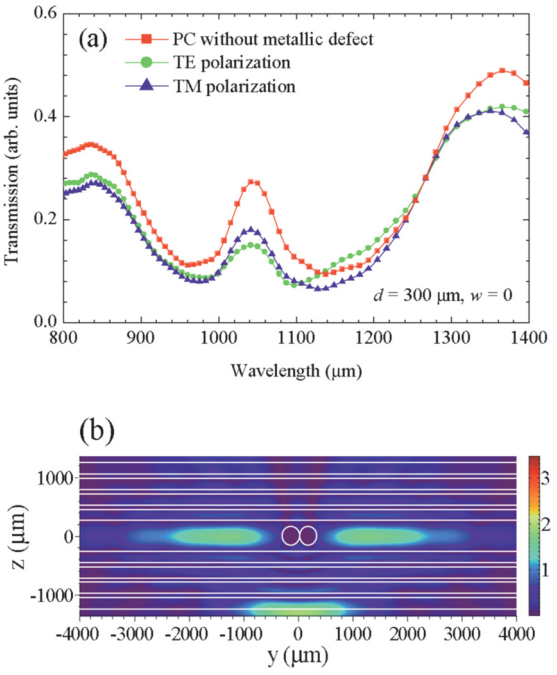

FIG. 12. (Color online) Measured transmission spectrum (a) and calculated electric field distribution of the PC containing two close-packed metallic wires ($d = 300$ μm, $w = 0$).

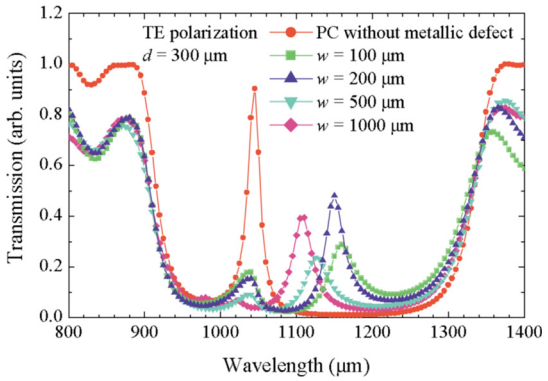

FIG. 13. (Color online) Evolution of the transmission spectrum of the PC containing two parallel metallic wires with increasing separation between the two metallic wires.

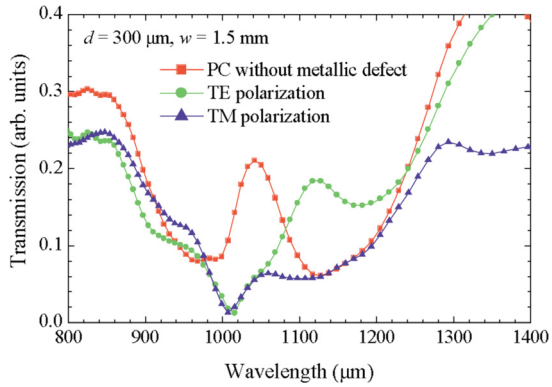

FIG. 14. (Color online) Measured transmission spectrum of the PC containing an array of four parallel metallic wires ($d = 300$ μm, $w = 1.5$ mm). The transmission spectrum of the PC without metallic wire is also provided for reference.

closely packed metallic wires ($w = 0$). In Fig. 12(a), we show the experimentally measured transmission spectrum of the 1D PC containing two closely packed metallic wires. For both TE- and TM-polarized waves, only a resonant mode is observed at the short-wavelength side. This situation is similar to that observed in the PC with a single metallic wire for TM-polarized waves. In this case, the dipole-like SPPs were not excited due to the large lateral size of the two closely packed wires. This behavior is confirmed by the electric field distribution calculated by FDTD simulation, which is shown in Fig. 12(b). It can be seen that the incident THz wave cannot be coupled into the wires through the excitation of SPPs. Instead, it is split into two identical parts when transmitting through the defect. As a result, the effective optical path is changed, leading to formation of the resonant mode at a shorter wavelength.

We have investigated by numerical simulation the effect of the separation between the two metallic wires on the appearance of the defect mode for TE-polarized waves. The result is shown in Fig. 13. When the separation between the two metallic wires becomes larger, the transmittance of the resonant mode at short wavelengths decreases while its peak remains nearly unchanged. In contrast, a blueshift is observed for the resonant mode at long wavelengths, which is related to SPPs. Its transmittance varies irregularly. The Q factor of this resonant mode is calculated to be ~30 and it is not sensitive to the separation between the two metallic wires.

VI. METALLIC DEFECT MODES FORMED BY FOUR PARALLEL METALLIC WIRES: EXPERIMENT

In the above experiments, the diameter of the metallic wire (in the case of single metallic wire) or the lateral dimension of the metallic wire arrays (in the cases of two widely separated or closely packed metallic wires) is smaller than the diameter of the THz beam. If we introduce an array of parallel metallic wires whose lateral dimension is comparable to or larger than the diameter of the THz beam, it is expected that the modification of the transmission spectrum will become more significant. In order to confirm this, we have employed an array of four parallel metallic wires separated by a distance of $w = 1.5$ mm. In this case, the lateral dimension of the array (~4.5 mm) is larger than the THz beam (~3.5 mm). In Fig. 14, we show the transmission spectra of the 1D PC containing four metallic wires for TE- and TM-polarized waves. For TE-polarized waves, only a resonant mode is found at the long-wavelength side of the original defect mode. At the short-wavelength side, one can see a deep transmission valley. For TM-polarized waves, only a deep transmission valley is observed at the short-wavelength side of the original defect mode. It implies that the transmission of TM-polarized waves is completely inhibited in this case. In fact, the array of metallic wires plays the role of metallic gratings, which can be employed as polarizers for THz wave.

VII. DISCUSSION

From the viewpoints of both fundamental research and practical application, it is important to clarify what will influence the Q factors of the metallic defects. For the air-gap defect, the Q factor of the resonant mode is calculated to be 52.3. When a 100 μm diameter metallic wire is inserted into the PC, the Q factor is slightly increased to 52.8 due to the shift of the resonant mode to a longer wavelength. For different metals such as Au, Ag, Al, Cu, and Pb, the parameters in the Drude model (i.e., the plasma frequency ω_p and the collision frequency Γ) are different in the THz spectral region.[31] The differences in these two parameters for different metals do not exceed a factor of 3.[31] In order to find out the influence of metal material on the Q factor of the metallic defect mode, we have examined the dependence of the Q factor of a single metallic wire on the parameters in the Drude model. The numerical simulation reveals that no obvious change is observed in the Q factor of the metallic defect mode when the two parameters are increased or decreased by one order of magnitude. Also, the change in the Q factor is negligible even the metal is assumed to be lossless. This result is consistent with the fact that metals resemble in many way a perfect conductor in the THz spectral region.[22] Therefore, the Q factor of the metallic defect mode is mainly limited by the loss of the glass slides constituting the PC and the coupling efficiency between the incident THz wave and the metallic defect mode.

When a single metallic defect created in a PC is employed to transmit a TE-polarized THz wave, the lateral dimension of the incident THz wave outside the PC is

dramatically reduced to the diameter of the metallic defect due to the strong localization of the SPP at the surface of the metallic defect. It implies that the incident THz wave can be focused to a feature size, which is eventually determined by the diameter of the metallic defect. More importantly, the lateral dimension of the THz wave is recovered after it transmits through the PC. Thus, the two perfect PCs (i.e., the two stacks of glass slides) on the two sides of the metallic defect behave as two focusing lenses that focus the parallel THz wave on the metallic defect and recover the focused wave to a parallel wave. As compared to the previous geometries proposed for the focusing of a THz wave, such as the use of tapered metallic waveguides or plasmonic parallel-plate waveguides,[22,32,33] the employment of metallic defects inserted in a PC enables the effective collection of the transmitted wave. This unique feature in combination with the small focusing size makes this geometry more attractive for the sensing of THz waves.[34]

VIII. CONCLUSION

We have investigated numerically and experimentally the transmission of THz waves through various metallic defects created by inserting single metallic wires or arrays of parallel metallic wires into the air-gap defect in a 1D PC. It is found that TE-polarized waves can transmit through metallic defects via excitation of SPPs. It is manifested in the formation of a resonant mode at the long-wavelength side of the original defect mode. For TM-polarized waves, the excitation of SPPs does not occur and the effect of the metallic wires is to split the incident THz wave into two identical parts. As a result, the corresponding defect mode is created at the short-wavelength side of the original defect mode. As for two parallel metallic wires, the appearance of the metallic defect mode depends strongly on the separation between the metallic wires. While the metallic defect mode for two widely separated metallic wires appears similar to that observed for single metallic wires, the excitation of dipole-like SPPs is prohibited for two close-packed metallic wires because of the large lateral size. For an array of four widely separated metallic wires whose lateral dimension is larger than the diameter of the THz beam, only the resonant mode related to the excitation of SPPs is observed for TE-polarized waves, and the transmission of TM-polarized is totally inhibited. Numerical simulation reveals that the confinement of the electric field in the propagation direction will facilitate the localization of the transverse SPP-related electric field at the surfaces of metallic wires. The experimental observations are in good agreement with the simulation results based on the FDTD technique. The metallic defects created in PCs may find applications in the focusing and sensing of THz wave.

ACKNOWLEDGMENTS

The authors acknowledge the financial support from the National Natural Science Foundation of China (Grant Nos. 10974060 and 11111120068), the project for high-level professionals in the universities of Guangdong province, and the Foundation for Distinguished Young Talents in Higher Education of Guangdong, China (Grant No. LYM10067).

[1] J. D. Joannopoulos, R. D. Meade, and J. N. Winn, *Photonic Crystals: Molding the Flow of Light* (Princeton University Press, Princeton, NJ, 1995).
[2] K. Inoue and K. Ohtaka, *Photonic Crystals: Physics, Fabrication: Applications* (Springer-Verlag, Berlin, 2004).
[3] J. S. Foresi, P. R. Villeneuve, J. Ferrera, E. R. Thoen, G. Steinmeyer, S. Fan, J. D. Joannopoulos, L. C. Kimerling, H. I. Smith, and E. P. Ippen, Nature (London) **390**, 143 (1997).
[4] A. Yariv, Y. Xu, R. K. Lee, and A. Scherer, Opt. Lett. **24**, 711 (1999).
[5] M. Bayer, T. Gutbrod, A. Forchel, T. L. Reinecke, P. A. Knipp, R. Werner, and J. P. Reithmaier, Phys. Rev. Lett. **83**, 5374 (1999).
[6] S. Lan, S. Nishikawa, H. Ishikawa, and O. Wada, J. Appl. Phys. **90**, 4321 (2001).
[7] P. R. Villeneuve, D. S. Abrams, S. Fan, and J. D. Joannopoulos, Opt. Lett. **21**, 2017 (1996).
[8] S. Lan, A. V. Gopal, K. Kanamoto, and H. Ishikawa, Appl. Phys. Lett. **84**, 5124 (2004).
[9] X. Y. Hu, Q. H. Gong, Y. H. Liu, B. Y. Cheng, and D. Z. Zhang, Appl. Phys. Lett. **87**, 231111 (2005).
[10] X. Y. Hu, P. Jing, C. Y. Ding, H. Yang, and Q. H. Gong, Nature Photon. **2**, 185 (2008).
[11] H. Y. Liu, S. Lan, L. J. Wu, Q. Guo, W. Hu, S. H. Liu, X. S. Lin, and A. V. Gopal, Appl. Phys. Lett. **90**, 213507 (2007).
[12] H. Němec, L. Duvillaret, F. Garet, P. Kužel, P. Xavier, J. Richard, and D. Rauly, J. Appl. Phys. **96**, 4072 (2004).
[13] H. Němec, P. Kužel, L. Duvillaret, A. Pashkin, M. Dressel, and M. T. Sebastian, Opt. Lett. **30**, 549 (2005).
[14] C. M. Yee and M. S. Sherwin, Appl. Phys. Lett. **94**, 154104 (2009).
[15] A. L. Bingham and D. Grischkowsky, Opt. Lett. **33**, 348 (2008).
[16] T. Hasek, H. Kurt, D. S. Citrin, and M. Koch, Appl. Phys. Lett. **89**, 173508 (2006).
[17] P. Mounaix, E. Freysz, J. Degert, N. Daro, J.-F. Létard, P. Kužel, V. Vigneras, and L. Oyenhart, Appl. Phys. Lett. **89**, 174105 (2006).
[18] J. Li, J. He, and Z. Hong, Appl. Opt. **46**, 5034 (2007).
[19] D. X. Qu, D. Grischkowsky, and W. L. Zhang, Opt. Lett. **29**, 896 (2004).
[20] W. L. Zhang, A. K. Azad, and J. G. Han, J. Z. Xu, J. Chen, and X. C. Zhang, Phys. Rev. Lett. **98**, 183901 (2007).
[21] P. R. Villeneuve, S. Fan, and J. D. Joannopoulos, Phys. Rev. B. **54**, 7837 (1996).
[22] S. A. Maier, S. R. Andrews, L. Martín-Moreno, and F. J. García-Vidal, Phys. Rev. Lett. **97**, 176805 (2006).
[23] K. J. Chau, G. D. Dice, and A. Y. Elezzabi, Phys. Rev. Lett. **94**, 173904 (2005).
[24] Y. Zheng, A. Johnson, E. Pyde, and K. J. Chau, Appl. Phys. Lett. **96**, 211111 (2010).
[25] C. J. E. Straatsma, M. A. Startsev, and A. Y. Elezzabi, J. Infrared Millim. Terahz. Waves **31**, 659 (2010).
[26] S. Liang, H. Y. Liu, Q. F. Dai, L. J. Wu, S. Lan, and A. V. Gopal, J. Appl. Phys. **109**, 024902 (2011).
[27] H. B. Liu and X. C. Zhang, "Terahertz Spectroscopy for Explosive, Pharmaceutical, Biological Sensing Applications," in *Terahertz Frequency Detection and Identification of Materials and Objects*, edited by R. E. Miles, X. C. Zhang, H. Eisele, and A. Krotkus (Springer, New York, 2007), pp.251–323.
[28] S. S. Harsha, N. Laman, and D. Grischkowsky, Appl. Phys. Lett. **94**, 091118 (2009).
[29] In this paper, a comercially available software developed by Rsoft Design Group (http://www.rsoftdesign.com) is used for the numerical simulations.
[30] M. A. Seo, H. P. Park, S. M. Koo, D. J. Park, J. H. Kang, O. K. Suwal, S. S. Choi, P. C. M. Planken, G. S. Park, N. K. Park, Q. H. Park, and D. S. Kim, Nature Photon. **3**, 152 (2009).
[31] M. A. Ordal, L. L. Long, R. J. Bell, S. E. Bell, R. R. Bell, R. W. Alexander, Jr., and C. A. Ward, Appl. Opt. **22**, 1099 (1983).
[32] V. Astley, R. Mendis, and D. M. Mittleman, Appl. Phys. Lett. **95**, 031104 (2009).
[33] H. Zhan, R. Mendis, and D. M. Mittleman, Opt. Express **18**, 9643 (2010).
[34] M. Theuer, R. Beigang, and D. Grischkowsky, Appl. Phys. Lett. **97**, 071106 (2010).